International Journal of Pharmaceutics 647 (2023) 123517

Contents lists available at ScienceDirect

International Journal of Pharmaceutics

journal homepage: www.elsevier.com/locate/ijpharm

Utilizing a microfluidic platform to investigate drug-eluting beads: Binding and release of amphiphilic antidepressants

Marcus Wanselius, Yassir Al-Tikriti, Per Hansson *

Department of Medicinal Chemistry, Uppsala University, BMC P.O. Box 574, SE-751 23 Uppsala, Sweden

ARTICLE INFO

Keywords:
Microgel
Microbead
Amphiphilic drug
Drug delivery
Microfluidics
Drug loading
Drug release

ABSTRACT

Drug-eluting beads made of responsive polyelectrolyte networks are used in the treatment of liver cancer. Aggregates of loaded drugs in complex with the networks dissolve upon release, causing swelling of the network. According to a recent mechanism the release and swelling rates are controlled by the mass transport of drug through a depletion layer created in the microgel. We hypothesise that the mechanism, in which the stability of the drug aggregates and the swelling properties of the network play crucial roles, offers means to control the release profile also for other drugs. To test this, we investigated the loading and release properties of amitriptyline, chlorpromazine and doxepin in polyacrylate, hyaluronate and DCbead™ microgels in a microfluidic setup. Loaded drugs could be released to a medium with physiological ionic strength and pH. The binding strength increased with decreasing critical micelle concentration of the drugs and increasing linear charge density of network chains. Microgels displayed drug-rich core/swollen shell coexistence, and swelled during release at a rate in agreement with the depletion layer mechanism, indicating its generality. The results demonstrate the potential of microgels as vehicles for amphiphilic drugs and the usefulness of the microfluidics method for *in vitro* studies of such systems.

1. Introduction

As a response to the ever-growing amounts of biologically-based pharmaceuticals, which to this day are still difficult to administer orally, there is a large focus on developing advanced delivery systems for parenteral delivery (Patel et al., 2014; Jain et al., 2019; Schwendeman et al., 2014; Zhang et al., 2013). An interesting type of drug delivery system is microgels. They consist of polymer networks and come in sizes ranging from colloidal microgels less than 1 μm in diameter to large microgels up to 500 μm in diameter (microbeads) (Murray and Snowden, 1995; Ran, 2017; Lewis and Dreher, 2012; Lewis and Holden, 2011; Hagan, 2019; Mikhail, 2022; Mikhail, 2021). The networks can be either charged or uncharged and designed to respond to changes in ionic strength, pH, or temperature by absorbing or releasing water (Karg, 2019; Saunders et al., 1997). In drug delivery, it is often desirable that they can reversibly bind large amounts of oppositely charged drug molecules, offer a protective aqueous environment for the drug molecules, (Malmsten et al., 2010) and enable controlled release of the bound drug (Eichenbaum et al., 1999; Vinogradov, 2006; Wechsler, 2019; Lengyel et al., 2019; Narayanaswamy and Torchilin, 2019; am Ende and Peppas, 1997; Siepmann and Siepmann, 2012; Censi et al., 2012; Kim et al., 2005; Cleland et al., 1997; Ahmad et al., 2021). Trans-arterial chemo-embolization (TACE) is an interesting example where these properties are taken advantage of for therapeutic purposes. DC bead™ is a microgel delivery system for doxorubicin and related drugs used in TACE treatment of liver cancer (Lewis and Holden, 2011). The drug loaded beads are deposited in the blood vessels feeding the tumour. During release, the beads increase their volume by absorbing water from the surroundings (Mikhail, 2022). The process leads to embolization, which is believed to be therapeutically advantageous in two ways. First, it reduces detrimental side effects by limiting systemic spreading of the drug. Second, it helps to kill the cancer cells by decreasing the supply of oxygen and nutrients to the tumour. The loading and release properties of the system have been investigated in detail. Lewis and co-workers showed that substantial amounts of doxorubicin can be loaded onto the beads when the ionic strength of the medium is low, a process during which the beads substantially decrease their volume (Lewis, 2006). Furthermore, the drug is released upon changing the medium to a drug-

Abbreviations: PA, polyacrylate microgels; DC, DC bead™; HA, hyaluronate microgels; DXP, doxepin hydrochloride; CPZ, chlorpromazine hydrochlorid; AMT, amitriptyline hydrochloride.

* Corresponding author at: Department of Medicinal Chemistry, Uppsala University, BMC P.O. Box 574, SE-751 23 Uppsala, Sweden.
E-mail address: per.hansson@ilk.uu.se (P. Hansson).

https://doi.org/10.1016/j.ijpharm.2023.123517
Received 30 June 2023; Received in revised form 25 September 2023; Accepted 15 October 2023
Available online 21 October 2023

free solution with physiological ionic strength, a process during which the beads increase their volume. Ahnfelt et al. made a comparative study of the loading and release of doxorubicin and a series of amphiphilic drugs (Ahnfelt, 2018). Their results show that doxorubicin's loading and release patterns were qualitatively the same as for the other drugs, all of which have well-documented self-assembling properties in aqueous solution. In particular, the drugs induced an osmotic collapse of the bead, transforming the water-swollen network into a dense phase made up from complexes between the drug and the oppositely charged network. Microscopy studies revealed that the beads displayed a core-and-shell morphology during loading and release, with the collapsed phase forming a shell growing at the expense of the swollen core network during loading, and the swollen network forming a shell growing at the expense of the collapsed core during release. Earlier it had been discovered that polyelectrolyte networks display the same type of behaviour when interacting with conventional micelle forming surfactants (Kabanov et al., 1997; Nilsson and Hansson, 2005).

Transformations between swollen and collapsed gel states are often referred to as volume phase transitions (VPT), a term originally used to describe phase transitions induced by temperature changes (Hansson, 2020; Tanaka, 1978). Various types of polyelectrolyte gels have been shown to undergo VPT's at a specific surfactant concentration in the solution denoted the critical collapse concentration (CCC). The transformation is accompanied by massive accumulation of surfactant micelles inside the gels, often arranged in ordered phases resembling the liquid crystalline phases found in concentrated surfactant solutions (Hansson, 1998; Khandurina et al., 1994; Yeh et al., 1998). The collapsed gel structures are believed to be stabilized by the electrostatic attraction between the micelles and the oppositely charged network chains, which has successfully been modelled as an attractive force between micelles mediated by the polyion chains (Gernandt and Hansson, 2015; Gernandt and Hansson, 2016). However, it is generally accepted that the major driving forces behind surfactant binding to gels are, first of all, the hydrophobic effect promoting self-assembly of the surfactant, and secondly, the entropic gain from the ion exchange reaction between the surfactant and network counterions leading to a more uniform distribution of the latter in the system. The entropic effect decreases with increasing salt concentration, explaining why the addition of salt destabilizes the complexes and promotes the release of surfactant.

Ahnfelt et al. proposed a mechanism in which the drug release rate is determined by the diffusive mass transport of drug molecules through the swollen shell network ("depletion layer") (Ahnfelt, 2018). The authors showed that the release rate, including that of doxorubicin, increased with increasing critical micelle concentration (CMC) of the drugs. This supported the proposed mechanism, according to which the concentration gradient in the shell, and hence the release rate, should increase with increasing concentration of drug monomers at the core–shell boundary, which is expected to be related to (but not equal to) the CMC. Recently, Al-Tikriti and Hansson developed a quantitative model based on the mechanism, taking into account the swelling of the microgel network, and showed that it accounted for the swelling rate of polyacrylate (PA) microgels releasing amitriptyline (Al-Tikriti and Hansson, 2020).

The results from previous work suggest that charged microgel beads can potentially be used as delivery systems for amphiphilic drugs in therapies other than TACE. To make way for that, we extend in this work the previous studies to include, in addition to DC bead™ and PA microgels, also microgels made from covalently cross-linked hyaluronic acid (HA). We test the generality of previous results by conducting a comparative study of the loading and release of the amphiphilic drugs amitriptyline, doxepin and chlorpromazine. The experiments are carried out by means of a microfluidics-based method specially designed for microgel studies. The method was recently developed in our lab as an *in vitro* method for investigations of interactions between peptide drugs and biopolymers of the extracellular matrix in subcutaneous tissue (Wanselius, 2022). In this work we aim to demonstrate its usability as an *in vitro* method also for investigations of microgel drug delivery systems.

2. Materials and methods

2.1. Chemicals and gels

Sodium phosphate monobasic (ReagentPlus ≥ 99 %), sodium phosphate dibasic (ReagentPlus ≥ 99 %), sorbitane monostearate (Span 60, S7010), amitriptyline hydrochloride (A8404), doxepin hydrochloride, chlorpromazine hydrochloride, lithium phenyl-2,4,6-trimethylbenzoylphosphinate (LAP, 900889), Sigmacote®, sodium chloride (NaCl, ≥99), sodium hydroxide (NaOH, ≥97 %), HOBt (1-hydroxybenzotriazole hydrate) (≥97.0 %), *N*,*N*,*N*′,*N*′-tetramethylethylenediamine (TEMED) (ReagentPlus 99 %), acetonitrile (anhydrous 99.8 %), ammonium persulfate (powder ≥ 98 %), acrylic acid (anhydrous 99 %), and *N*,*N*′-methylenebisacrylamide (99 %) were all acquired from Sigma Aldrich, SE. Sodium hyaluronate (100–300 kDa) was purchased from Contipro a.s (Dolní Dobrouč, CZ), and DC Bead™ (70–150 μm) was from Biocompatibles UK Ltd (Surrey, UK). Novec™ 7500 (>99 %) was purchased from 3 M (Saint Paul, MN, USA) and Picosurf™ 5 % in Novec™ 7500 was acquired from Sphere fluidics (Cambridge, UK). Polydimethylsiloxane (PDMS) DowSyl Sylgard™ 184 including the elastomer base and curing agent were from GA Lindberg ChemTech AB (Stockholm, SE). EDC (N-(3-dimethylaminopropoyl)-N'-ethylcarbodiimide hydrochloride was purchased from Acros Organics, (Geel, BE). N-(2-aminoethyl) acrylamide hydrochloride was from abcr GmbH (Karlsruhe, GE), and Spectra/Por® 6 RC-membrane (3.5 kDa cutoff) was from SpectrumLabs (Rancho Dominguez, CA, USA). SUEX photoresist film was from DJ MicroLaminates (Sudbury, MA, USA). 2-propanol (ACS reagent) was purchased from Merck KGaA (Darmstadt, GE) and ethanol (99.7 %) was from Solveco (Rosersberg, SE). mr-Dev 600 development solution was from micro resist technology GmbH (Berlin, GE). Deionized (DI) water (Millipore Synergy with UV ultrapure, type 1, water purification system, 18.2 MΩ cm at 25 °C, from Merck KGaA (Darmstadt, GE))

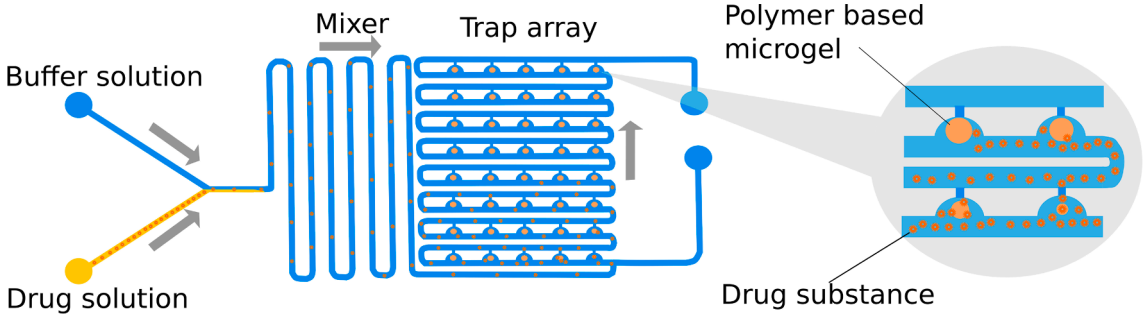

Fig. 1. Illustration of a microfluidic chip used for interaction studies (MIS) not according to scale; arrows indicate the flow direction. (1) Inlet for solvent, (2) inlet for solution of drug molecule, (3) mixer for complete mixing of the solvent and stock solution, (4) inlet for microgels, (5) 96 single-microgel traps of 200 μm diameter, (6) outlet for liquid. Reused with permission from (Wanselius, 2022).

were used for all aqueous solutions. All chemicals were used as received.

The standard aqueous medium used for all experiments in this work contained 7 mM sodium phosphate monobasic and 3 mM sodium phosphate dibasic as a buffer system. The pH was adjusted to 7.4 or 5.9 by adding small amounts of HCl. As release medium we used the pH 7.4 phosphate buffer with 150 mM NaCl added. The buffers are referred to as PB pH 7.4 and PB pH 5.9 in this work.

2.2. Microgel fabrication

PA microgels were synthesized by using an inverse suspension polymerization technique and the crosslinker N,N′-methylenebisacrylamide (corresponding to 1.4 mol% of the total amount of acrylic acid monomers); the full process has been described previously (Al-Tikriti and Hansson, 2020). The diameter of the PA microgels was within the range of 100–200 μm in PB pH 7.4.

HA microgels were fabricated in two steps. First, linear hyaluronic acid was modified with N-(2-aminoethyl) acrylamide hydrochloride to a modification degree of 13 %. The acrylamide-modified hyaluronic acid was then dissolved into water (2 wt%) and crosslinked into spherical microgels with the use of a droplet-making microfluidic chip. A detailed description has been presented by Wanselius (2022). The final size of the microgels was within the range of 140–180 μm in diameter in PB pH 7.4.

2.3. Microfluidic chip fabrication

The fabrication of microfluidic chips used in this work was performed with standard soft lithography techniques, this process has also previously been described in detail (Wanselius, 2022). Both the microfluidic chip for droplet production (MDP) used during HA microgel fabrication and the microfluidic chip for interaction studies (MIS) were made of PDMS. A schematic of the MIS is presented in Fig. 1.

2.4. Determination of microgel volume

Microgel volumes during experiments were determined by measuring the diameter of the gels and then calculating the volumes assuming fully spherical microgels. Diameters were measured using an Olympus BX51 microscope equipped with an UMPlanFI 5 × lens and an Olympus DP73 digital camera together with the imaging software cellSens Dimension version 1.7.1 all from the Olympus Corporation (Tokyo, JP).

2.5. Charge concentration determination of HA microgels

A dispersion of spherical HA microgels in water was placed in a small sealed microscopy cell designed in our lab (Al-Tikriti and Hansson, 2022). The radius of all microgels was measured by using the Olympus Bx-51 light microscope setup. These microgels were then freeze-dried and weighed by a Mettler Toledo MT5 microbalance (Columbus, OH, USA). In addition, differential scanning calorimetry instrumentation (DSC Q 2000, TA instruments (New Castle, DE, USA)) was used to measure the remaining moisture content after freeze-drying to obtain the correct weight. The average charge concentration was calculated based on the weight of HA microgels, the degree of modification, and the total volume of the microgels.

2.6. Interaction experiments in the MIS

The MIS (Fig. 1) used for interaction studies in this work was connected to a pressure pump setup from Elveflow (Paris, FR) including the OB1 MK3 + flow controller with associated MFS flow sensors and a MUX 12 distributor. The chip was connected to the setup with Masterflex tubing (EW-06417–11) with an inner diameter of 300 μm. Flow was controlled with software developed for the pressure pump (ESI).

Microgels were loaded into the microfluidic chip through an inlet dedicated for microgels and one microgel was contained in each of the 96 half-circled shaped hydrodynamic traps. The loading took place during a constant flow of DI water. Before each experiment, the diameter of the gels in the buffered solutions used for loading and release, respectively, were measured. The experiments were then performed in two steps. First each gel type (HA, PA, and DC) was exposed to each amphiphilic drug (AMT, DXP, CPZ) at different concentrations to estimate the critical aggregation concentration (CAC) and the critical collapse concentration (CCC). During this step, the exposure time to each concentration was relatively short, ranging from 10 to 30 min. CAC is defined as the concentration in the liquid solution at which micelles start to form inside the microgels. This was taken as the concentration in the medium required to detect a volume change of the gel substantially larger than that produced by simple salts (e.g., NaCl) at the same concentration. CCC is defined as the concentration in the solution where a volume phase transition (VPT) of the microgel network takes place (Gernandt and Hansson, 2015; Sasaki et al., 2001). To investigate the kinetics of the volume change induced by the selected drugs, microgels were exposed, in turn, to at least two drug concentrations above CAC. The deswelling process was monitored by taking microscopy images of the microgels as they evolved from the swollen drug-free state to the collapsed drug-loaded state. From the images, the diameter and internal morphology of the microgels were determined, and graphs of the relative gel volume as a function of time were constructed, assuming a spherical gel shape. At the end of each loading experiment, the medium inside the microfluidic chip was changed to a release medium (PB pH 7.4, 150 mM NaCl) causing a dissolution of micelles and release of the drug molecules from the microgels. During the release of the drug molecules, the morphology and volume change was once again recorded.

2.7. MIS data analysis

We use mathematical models of the kinetics of drug mediated microgel deswelling and swelling to analyse experimental data. The models are based on the assumption that drug mass transport is overall rate controlling for the microgel volume changes observed upon drug loading and release. The models have been derived and evaluated elsewhere (Ahnfelt, 2018; Al-Tikriti and Hansson, 2020; Wanselius, 2022).

Microgel deswelling rate during drug loading. Earlier works show that the rate of volume change of microgels undergoing VPT induced by an amphiphile is, in general, controlled by mass transport of the amphiphile to the microgel surface (film control) or inside the microgel (particle control) (Nilsson and Hansson, 2005; Nilsson and Hansson, 2007; Nilsson and Hansson, 2008). To determine which process dominates, we fit a model valid for film control to experimental data, and compare the diffusion coefficient of the drug D obtained from the fit with the diffusion coefficient taken from literature. According to the model, (Ahnfelt, 2018) the microgel volume V relative to that prior to binding V_0 is given by:

$$\frac{V(t)}{V_0} = (1 - kt)^{3/2} \tag{1a}$$

$$k = \frac{ShD(\bar{v}_0 - \bar{v}_S)f_S\Delta C}{2R_0^2} \tag{1b}$$

where Sh is the Sherwood number, $\bar{v}_0$ is the volume per mole of network charges for a drug-free microgel in equilibrium with the liquid, $\bar{v}_S$is the local volume per moles of network charged groups in the shell, f_S is the network-to-drug charge ratio in the shell, R_0 is the radius of a drug-free microgel in equilibrium with the liquid, and $\Delta C = C^{liq} - CAC$, where C^{liq} is the drug concentration in the liquid and CAC (critical association concentration) is the lowest concentration in the liquid at which drug self-assemblies in the microgel can be detected at equilibrium (see below

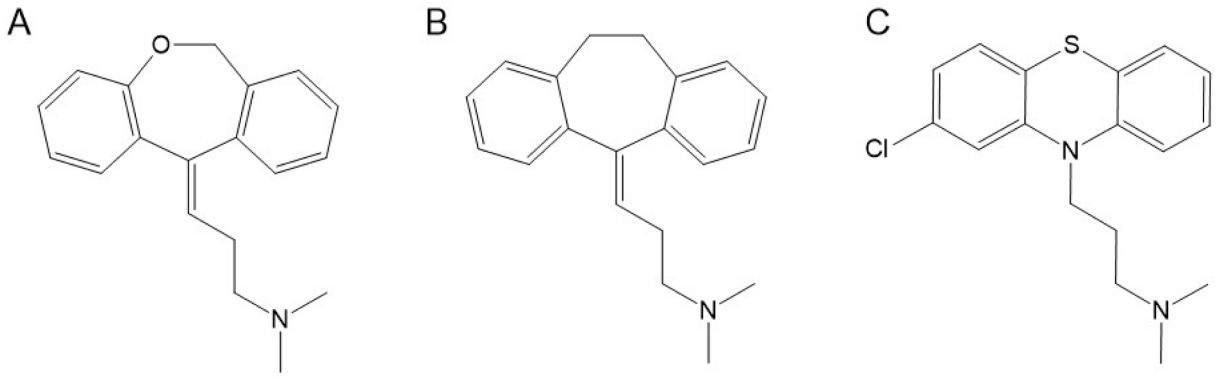

Fig. 2. Molecular structures of A) doxepin B) amitriptyline C) chlorpromazine.

and Supplementary materials for details).

Microgel swelling rate during drug release. We use a model proposed by Al-Tikriti and Hansson to analyse the kinetic data (Al-Tikriti and Hansson, 2022). The model describes the swelling of a microgel undergoing VPT upon the release of an amphiphilic drug to a medium acting as a sink by means of (quasi-) steady-state kinetics. During the process the microgel contains a dense core of radius r_{in} filled with drug micelles, and a micelle-free swollen shell of outer radius r_{out}. The time t to increase the fraction of network in the shell q_S from zero to q_{St} is (adapted to the notations used here):

$$t = \frac{\beta_C R_0^2}{3\bar{v}_C D'} \int_0^{q_{St}} \frac{1}{C'_{in}} \left(\frac{R_0}{r_{in}} - \frac{R_0}{r_{out}} \right) dq_S \tag{2}$$

where R_0 is the radius of the microgel in equilibrium the drug-free release medium, D' is the diffusion coefficient in the shell, C'_{in} is the concentration of drug in the shell at the core–shell boundary, and β_C is the drug/network charge ratio in the core, as distinct from the average drug/network charge ratio in the microgel β.

$$\frac{R_0}{r_{in}} = \left(\frac{\bar{v}_0}{\bar{v}_C(1-q_S)} \right)^{\frac{1}{3}} \tag{3a}$$

$$\frac{R_0}{r_{out}} = \left(\frac{\bar{v}_0}{\bar{v}_C(1-q_S) + \bar{v}_S q_S} \right)^{\frac{1}{3}} \tag{3b}$$

When applying the model in this work, we put $\bar{v}_C$ = constant and $C'_{in} = C^0_{in}(1 - aq_S)$. Eq. (2) then becomes:

$$t = \frac{\beta_C R_0^2 \bar{v}_0^{1/3}}{3\bar{v}_C^{4/3} D' C^0_{in}} \int_0^{q_{St}} (1-aq_S)^{-1} \left\{ (1-q_S)^{-1/3} - \left(1 - q_S + \frac{\bar{v}_S}{\bar{v}_C} q_S \right)^{-1/3} \right\} dq_S \tag{4}$$

where C^0_{in} and a are system specific constants. Justification of Eq. (4) is provided as Supplementary material (S1), where we also show that $\bar{v}_S/\bar{v}_C$ as a function of q_S is little dependent on $\bar{v}_C$ and the parameters determining the deformation and swelling of the network (S2).

3. Physicochemical properties of amphiphilic drugs and microgels

Fig. 2 shows the chemical structure of the three antidepressant drugs investigated in this work: doxepin, amitriptyline, and chlorpromazine. All three were added to the systems as hydrochloride salts, and we denote them DXP, AMT, and CPZ, respectively, when referring to them in that form. All three have a non-polar part consisting of a tricyclic aromatic group attached via a short hydrocarbon chain to a dimethyl ammonium group. Being weak acids with $pK_a \gtrsim 9$, a large fraction of the ammonium groups are expected to be protonated when dissolved in water. The ionized forms, with a large hydrophobic moiety connected to a hydrocarbon chain carrying a charged, terminal nitrogen atom, are clearly amphiphilic. AMT and CPZ have been shown to effectively lower the surface tension of aqueous solutions, and plots of surface tension *vs.* concentration display break points indicative micelle formation at distinct CMC values (Efthymiou et al., 2021). For AMT, the formation of proper micelles has been confirmed by SAXS measurements, showing that the aggregation number varies between 32 and 42 for concentrations between 0.09 and 1.1 M (Efthymiou et al., 2021). For CPZ, aggregation numbers between 21 of 42 has been reported for concentrations between 0.03 and 0.4 mol/kg from SANS measurements in D_2O (Perez-Villar et al., 1993). Likewise, for DXP, a CMC and aggregation numbers have been reported from light scattering measurements (Attwood and Gibson, 1978). In Table 1, we have collected physicochemical properties of the hydrochloride salts in aqueous solution, taken from the literature. Based on the CMCs, the hydrophobicity increases as DXP < AMT < CPZ. The chemical structures suggest that replacing an oxygen atom with a carbon atom increases the hydrophobicity (DXP → AMT), and replacing three carbon atoms with nitrogen, sulphur and chlorine further increases the hydrophobicity (AMT → CPZ), in agreement with expectations. Efthymiou et al. (2021) have argued that at low concentrations in water, the micelles contain a mixture of the uncharged base form and the ionized form, but that the fraction of the latter increases with increasing concentration because of a simultaneous lowering of the pH of the solution. Another factor is that, decreasing the concentration tends to decrease the degree of ionization of the drug molecules in the micelles because the positive electrostatic potential at the micelle surface tends to increase with decreasing concentration. In the present work, where the added buffer maintains the

Table 1
Physicochemical properties of AMT, DXP, and CPZ.

Drug (HCl salts)	CMC (mM)	Molecular Weight (g/mol)	pKa	D_{H_2O} (x 10^{-6}cm^{2}s^{-1})
Amitriptyline	36–43 (Efthymiou et al., 2021)	314	9.4 (Green, A.L., 1967)	6.95 (Attwood and Gibson, 1978)
Doxepin	62 (Attwood and Gibson, 1978; Attwood and Natarajan, 1983)	316	8.96 (Embil and Torosian, 1982)	7.07 (Attwood and Gibson, 1978)
Chlorpromazine	16–22 (Efthymiou et al., 2021; Attwood and Gibson, 1978; Attwood and Natarajan, 1983)	355	9.3 (Ijzerman, 1988)	6.92 (Attwood and Natarajan, 1983)

Table 2
Charge properties and radius (R_0) in PB of HA, PA, and DC.

Microgel	Charge concentration, C_p^0(mM)	Linear separation of charges, b (Å)	Microgel radius, R_0 (μm)[b]
PA	90 (Al-Tikriti and Hansson, 2020)	2.5	75–85
DC	60 (Ahnfelt, 2018)	2.5 (PAMPS)	65–95
HA	30	12 [a]	75–80

[a] Ethyl acrylamide modified HA (13% modification degree).
[b] In PB pH 7.4.

pH value close to 7.4, the degree of ionization is expected to be high in the liquid solutions in contact with the microgels. Furthermore, for micelles residing inside the microgels, the degree of ionization is expected to be close to unity as long as the negative charge from the network is larger than the positive charge from the drug molecules, because hydrogen ions will be enriched inside the microgels due to the mean negative electrostatic potential. Finally, we note that the hydrochloride salts of all drugs have about the same diffusion coefficient (D_{H_20}) in water, which is reasonable considering the similarity in molecular structure.

The microgels were chosen to cover a range of properties (Table 2). PA and HA microgels both consist of a single type of flexible covalently cross-linked polymer; PA consist of sodium polyacrylate while HA are made of ethyl acrylamide-modified sodium hyaluronate chains. PA is a highly charged, flexible, and hydrophilic polymer. In comparison, the HA backbone is bulkier, less flexible, and has a considerably lower linear charge density (even slightly lower than native HA due to the ethyl acrylamide modification). DC bead™ is made up of a covalently cross-linked hybrid network of uncharged polyvinyl alcohol (PVA) chains and poly(2-acrylamido-2-methylpropanesulfonate) chains (PAMPS) of high negative charge density (Lewis, 2006). All three microgels are expected to mainly interact electrostatically with the amphiphilic drugs. The networks are highly responsive and typically display large collapse amplitudes upon binding of oppositely charged proteins and self-assembling amphiphiles (Wanselius, 2022). However, the density of the collapsed state for DC bead™ appears to be affected by the positive contribution to the osmotic swelling pressure from PVA.

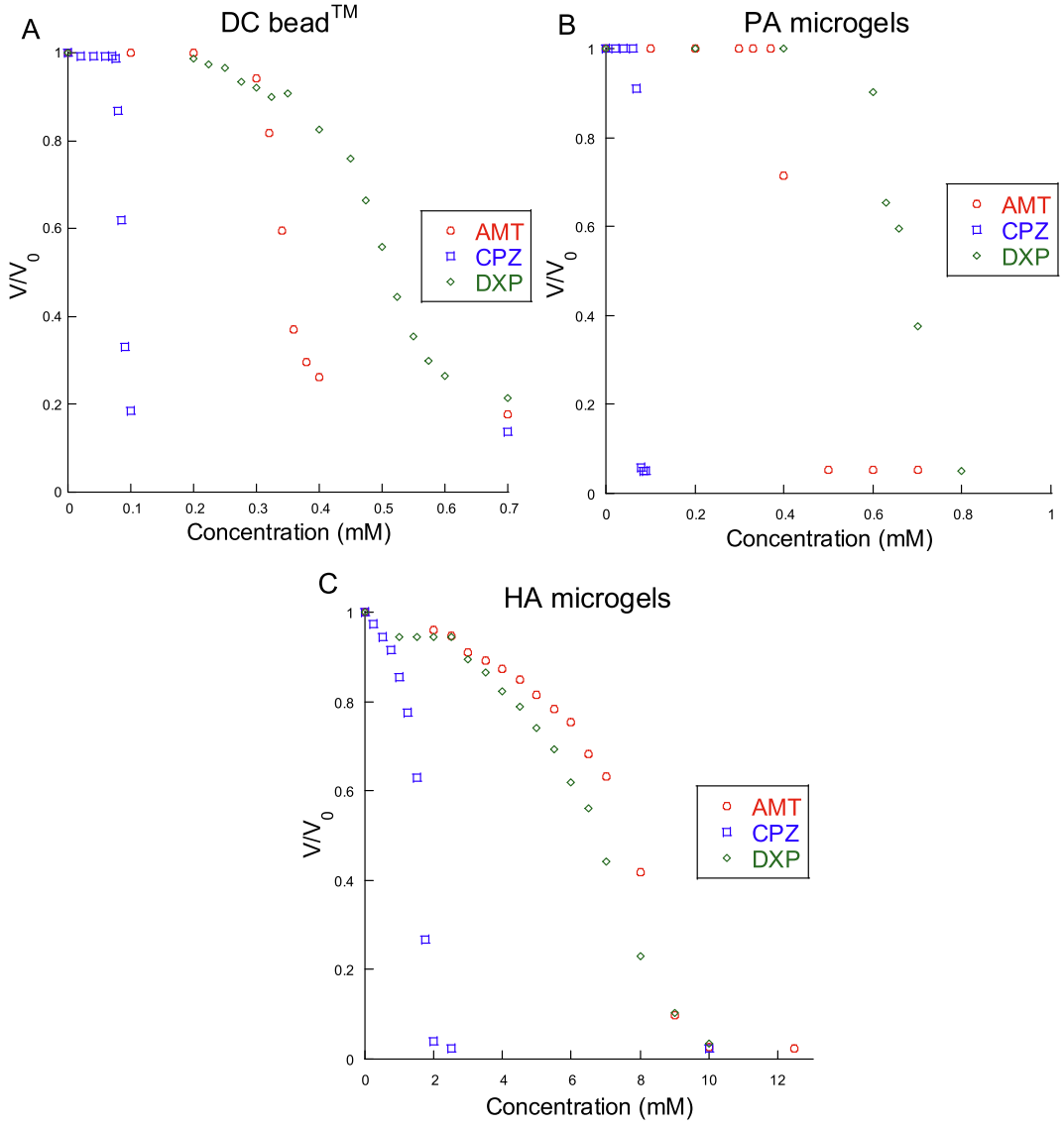

Fig. 3. Volume change of DC (A), PA (B), and HA (C) at exposure to different concentrations of AMT, DXP, and CPZ. The exposure time to each concentration is 10 min.

Table 3
Values of CAC and CCC (measured), and of C_{liq}^{end}, and C_{p}^{end}(calculated) for the microgel-drug systems in this work.

System	CAC (mM)	CCC (mM)	C_{liq}^{end} (mM)	C_{p}^{end} (M)
DC/AMT	0.3	(0.3)	0.5	0.33
DC/DXP	0.3	–	0.6	0.24
DC/CPZ	0.07	(0.07)	0.09	0.33
PA/AMT	0.4	0.4	0.4	1.5
PA/DXP	0.5	–	0.8	1.9
PA/CPZ	0.06	0.07	0.08	1.9
HA/AMT	(1)	–	10	1.1
HA/DXP	2	–	10	1.1
HA/CPZ	0.4	(1.5)	2	1.5

4. Results and discussion

4.1. Microgel - drug solution equilibria at low ionic strength

In this section we show how the swelling of PA, DC and HA microgels varied with the concentration of respectively AMT, DXP, and CPZ in the liquid solution at equilibrium. The experiments were carried out with the MIS setup in buffered solutions with low ionic strength (10 mM PB pH 7.4) ("loading conditions"). Since the solution flowing through the microchip was constantly renewed, the microgels were in contact with a medium of constant drug concentration/fixed chemical potential ("solution reservoir").

Fig. 3A-C show microgel swelling isotherms, i.e., plots of the ratio V/V_0 as a function of the drug concentration, where V is the actual volume and V_0 is the volume in the buffered solution without drug. In all systems, the volume decrease caused by the drug was ca. 80 % or larger. For comparison, the volume decrease caused by the addition of 10 mM NaCl is only ca. 20 %, an effect mainly ascribed the increased ion concentration/osmotic pressure in the solution (Wanselius, 2022). The large deswelling observed here shows that the drugs formed micelle-like aggregates inside the microgels. As discussed in detail elsewhere, there are mainly two contributions to the effect (Gernandt and Hansson, 2016; Hansson, 2009; Khokhlov et al., 1992). The first is explained by translational entropy: A micelle of aggregation number N replaces N network counterions, thereby lowering the concentration of mobile species in the microgel, and with that the osmotic swelling pressure in the microgel decreases. In response to that, the network contracts elastically until the osmotic equilibrium with the solution is re-established. The other contribution is due to electrostatic free energy: The network polyion chains interact more strongly with multivalent species like a charged micelle, than with monovalent counterions, thereby giving rise to stronger cohesive forces stabilising the collapsed gel state. Because both contributions should increase in magnitude with increasing aggregation number, so should the rate of volume change with increasing drug concentration (cooperative effect). For all systems in Fig. 3, the swelling isotherms started to bend downward rather abruptly in a concentration range narrow enough to warrant the determination of a critical aggregation concentration (CAC), indicating the onset of micelle formation in the microgels. In most cases the deswelling proceeded continuously with increasing concentration until the microgel volume reached a plateau at a rather well defined drug concentration in the solution denoted C_{liq}^{end}. However, for PA in combination with AMT and CPZ, the swelling isotherms displayed a discontinuity at a critical collapse concentration (CCC), characteristic of a volume phase transition (VPT) of the microgel. In three more cases the volume change was very sharp, possibly indicating a VPT proceeding at a low rate, as further discussed later.

Table 3 shows the determined CAC, CCC and C_{liq}^{end} values. The CAC values follow the trend expected from the drugs' respective CMCs. Thus CPZ, which has the lowest CMC (Table 1), started to form micelles in all microgels at the lowest concentrations in the solution (lowest CAC), followed by, in turn, AMT and DXP. This is in agreement with results for series of conventional cationic surfactants with different hydrocarbon tail lengths (Nilsson and Hansson, 2007; Hansson, 2006). The result shows that the drugs interact in a similar way with each polyelectrolyte, and that the CACs differ mainly because of the difference in size of the non-polar group, as reflected by their respective CMCs. That CAC for CPZ is a magnitude smaller than for the other two while the CMCs differ by only a factor of two or three, is most likely an effect of how the electrostatic interactions affect the CMCs. Recall that, in the absence of extra added salt, the electrostatic interactions are very sensitive to the concentration of the drug itself, and thereby the electrostatic repulsion between the drug molecules in a micelle. Therefore, the CMC in pure water increases more slowly with decreasing hydrophobicity than the CMC determined in the presence of a fixed salt concentration (Evans and Wennerström, 1994). However, this cannot account for the fact that the HA swelling isotherms for AMT and DXP are very similar while the differences in CMC is large. At the moment, we are not able to explain that but an investigation of the aggregation numbers in the microgels could shed light on the problem.

Based on the CACs, the drugs interact nearly equally strong with DC and PA but much weaker with HA. This is in agreement with earlier studies of polyelectrolyte-surfactant systems and can be explained (Wanselius, 2022) by the much lower linear charge density of HA compared to that of the other two (Table 2). We have included in Table 3 also C_p^{end}, the concentration of network charged groups in the microgels at C_{liq}^{end}, calculated from the determined collapse amplitude and the microgel charge concentration in the swollen state C_0 (Table 2). The C_p^{end} values show that the collapsed gel states were more swollen for DC than for PA. This is explained by the uncharged PVA chains in DC contributing to the swelling pressure (see section 2.7), thereby prohibiting the gels from collapsing to a very dense state.

For systems that do not undergo VPT, the difference between CAC and C_{liq}^{end} provides a measure of the sharpness of the volume change. For PA and DC, the difference is smaller than for HA. The steeper slope indicates a higher cooperativity in the binding. We attribute this primarily to the electrostatic interactions between micelles and the network chains. Thus, when the drug binding ratio increases, the concentrations of both polyelectrolyte and micelles increase. Because the negatively charged polyion chains are on average brought closer to the positively charged micelle charges, the electrostatic free energy per bound drug molecule decreases, which explains why the process is cooperative. This type of cohesive interaction becomes stronger with increasing linear charge density of the network chains (and increasing micelle charge), (Gernandt and Hansson, 2016) explaining why the PA and DC swelling isotherms are steeper than the HA ones. It also suggests that DXP gives rise to less steep swelling isotherms than AMT and CPZ because DXP forms micelles with smaller aggregation number in the microgels. According to theory, when the polyion-mediated attractions between micelles are sufficiently strong the system may undergo a VPT at a critical surfactant concentration (CCC), where the energetically stabilised collapsed state at high binding ratio becomes favourable enough to compete with the entropy-favoured swollen state at low binding. However, the hydrophobic driving force behind micelle formation also promotes VPT (Andersson and Hansson, 2017; Tararyshkin et al., 2007). In this work there are examples of swelling isotherms displaying a VPT as well as cases where V/V_0 decreases continuously with increasing concentration, i.e., there is a CAC but no CCC. In systems displaying a VPT, experiments show that substantial amounts of micelles may be accumulated and uniformly distributed in the swollen gel states prior to VPT. However, even though CAC should be smaller than CCC, in practice they nearly coincide because the cooperativity of binding is large also prior to VPT. Results from thermodynamic model calculations show that the amount of micelles that gels can host without phase separating or undergo VPT decreases with increasing size of the non-polar part of the amphiphile, highlighting the importance of the hydrophobic driving force (Andersson and Hansson, 2017). For an overview of papers dealing

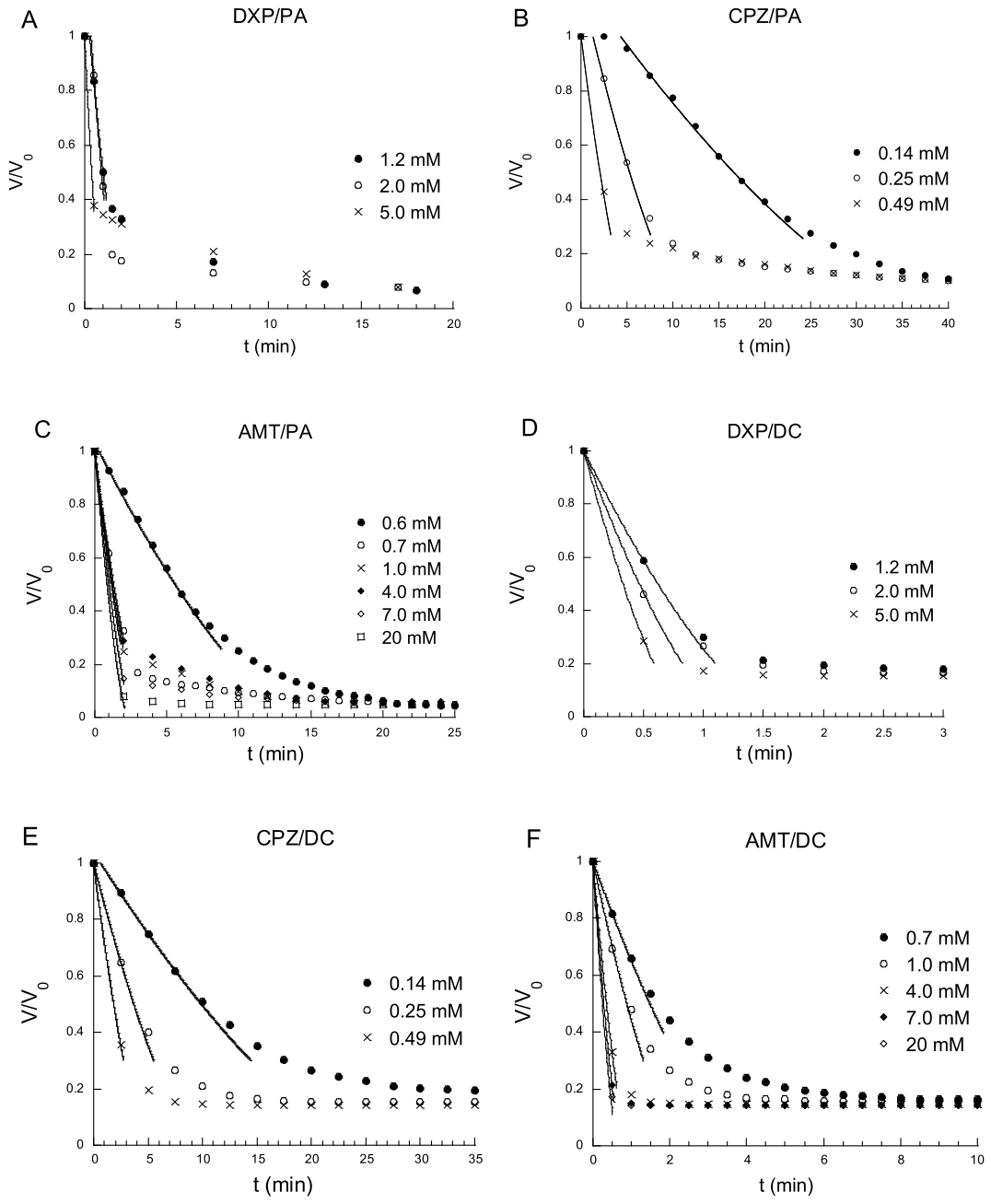

Fig. 4. The volume change of microgels over time at exposure to amphiphilic drug molecules. PA exposed to DXP (A), CPZ (B), and AMT (C). DC exposed to DXP (D), CPZ (E) and AMT (F). Liquid volume flow through microchip: 200 μl/min.

with that problem and factors determining whether microgels are phase separated or homogeneous, see ref. (Hansson, 2020).

Before closing this section, we emphasize that in some cases it was difficult to determine if the systems had reached equilibrium or not. For example, in the case of HA microgels exposed to AMT, the change of volume at each concentration was rapid, and the exposure time was long enough to reach equilibrium at each concentration. However, when the same microgels interacted with DXP solutions with concentrations near C_{liq}^{end}, the collapse was very slow and equilibrium may not have been reached during the exposure time of 10 min used in the experiment in Fig. 3C. Thus, it is possible that the kinetics masked the VPT, as will be further illuminated by theoretical calculations of mass transfer-controlled deswelling. In Table 3 we have put the CCC values within parentheses for systems where we believe this to be the case.

4.2. Deswelling kinetics upon drug binding

Fig. 4 shows V/V_0 as a function of time for PA and DC during exposure to solutions with different concentrations of the amphiphilic drugs; V is the actual volume and V_0 is the volume in PB (7.4) or (for AMT) PB (5.9) before drug exposure. The deswelling rate for all systems was strongly dependent on the concentration in the liquid solution, with a higher concentration resulting in a more rapid volume change. The behavior resembles that observed by Ahnfelt et al. during loading of amphiphilic drugs onto single DC microgels positioned in a liquid flow by means of micropipettes (Ahnfelt, 2018). The authors showed that Eq. (1) described well the shape of initial part of the deswelling curves, and how the deswelling rate depended on the drug concentration. Eq. (1) is based on the assumption that drug mass transport from the bulk liquid to the microgel surface controls the rate of deswelling of microgels

Table 4
Deswelling kinetics. Results from model fitting with Eq. (6).

System	$R_0(\mu m)$[a]	C^{liq}(mM)	k (min^1)	D_{app}(m^2/s)
DC/AMT	82	0.70	0.25	3×10^{-10}
	"	1.0	0.42	3×10^{-10}
	"	4.0	1.1	2×10^{-10}
	"	7.0	1.3	1×10^{-10}
	"	20	1.5	4×10^{-11}
DC/DXP	77	1.2	0.60	3×10^{-10}
	"	2.0	0.8	2×10^{-10}
	"	5.0	1.1	1×10^{-10}
DC/CPZ	79	0.12	0.60	4×10^{-10}
	"	0.25	0.80	3×10^{-10}
	"	0.49	1.1	2×10^{-10}
PA/AMT	75	0.60	0.070	2×10^{-10}
	"	0.70	0.28	6×10^{-10}
	"	1.0	0.32	3×10^{-10}
	"	4.0	0.30	5×10^{-11}
	"	7.0	0.37	3×10^{-11}
	"	20	0.43	1×10^{-11}
PA/DXP	85	1.2	0.50	6×10^{-10}
	"	2.0	0.65	3×10^{-10}
	"	5.0	0.95	2×10^{-10}
PA/CPZ	77	0.14	0.030	2×10^{-10}
	"	0.25	0.093	3×10^{-10}
	"	0.44	0.18	3×10^{-10}

[a] Average value based on 5 – 9 microgel species.

displaying core–shell separation during loading. To test if that type of film-control ("stagnant layer" diffusion) governs the process in our systems, we fitted the initial part of the deswelling profiles in Fig. 4 with Eq. (1a), using the "rate constant" k as fitting parameter. The solid curves in Fig. 4 represent the model fits. From the resulting k values we then used Eq. (1b) to calculate the apparent diffusion coefficient (D_{app}) of the drug in the liquid; both values are reported in Table 4. To obtain $D_{app,}$ we calculated ΔC from the actual drug concentration C^{liq} and CAC (Table 3), and $\bar{v}_0$ and $\bar{v}_S$ from C_p^0 (Table 2) and C_p^{end} (Table 3), respectively, for each system. We set$f_S = 1$, $Sh = 30$, and the initial microgel radius (R_0) equal to the average value for the different microgel species employed (Table 4). Sh was determined earlier for DC/AMT using the same setup and liquid flow rate as used here and should be relevant for all systems in this study because R_0 and D have about the same values in all systems (Wanselius, 2022). The diffusion coefficients in dilute aqueous solution (C < CMC) for the drug hydrochloride salts are given in Table 1. However, as described elsewhere, the relevant value describing the diffusive transport in the stagnant layer under the present conditions, is the diffusion coefficient of the drug cation, which can be calculated from the relationship $D_{1:1} = 2D_+D_-/(D_+ + D_-)$ valid for monovalent electrolytes, where D_+ is the diffusion coefficient of the cation and D_- is the diffusion coefficient of the anion (Al-Tikriti and Hansson, 2020). With$D_- = 2 \times 10^{-9}$ m^2/s (chloride ion) and $D_{1:1} = 7 \times 10^{-10}$ m^2/s for the hydrochloride salt (Table 1), we obtain a diffusion coefficient of 4×10^{-10} m^2/s, valid as an estimate for all three drug cations. As can be seen in Table 4, the apparent diffusion coefficients calculated from k obtained at the lowest drug concentrations are close to that value, indicating that stagnant layer diffusion largely controls the deswelling process. At higher drug concentrations, D_{app} decreases to values lower than expected for the drug cations in water, showing that other processes control the deswelling. Indeed, the results from detailed micropipette investigations of PA suggest a turnover from "film control" to "particle control" with increasing concentration (Nilsson and Hansson, 2005). In particular, the formation of dense shells imposes a diffusion barrier which slows down the deswelling and eventually becomes rate limiting as the shells grow thicker. Most likely, this is what causes the measured deswelling profiles to deviate from the simple law of Eq. (1) when V/V_0 falls below a certain value in Fig. 4, as pointed out elsewhere (Ahnfelt, 2018; Al-Tikriti and Hansson, 2020; Wanselius, 2022).

The tendency to undergo VPT and form densely packed outer shells during the collapse process is expected to increase with increasing linear charge density of the network chains. A core–shell behavior has visually been confirmed for all systems in this work, except HA exposed to drug concentrations close to C_{liq}^{end}. Because collapsed shells are very thin during large parts of the deswelling process, they are difficult to detect with light microscopy and can easily be missed when the collapse is fast (Nilsson and Hansson, 2005). However, shells of thickness comparable to the wavelength of visible light reveal themselves by the coloured reflections appearing at the rim of the microgels. As an example, Fig. 5 shows microscopy images of a PA microgel undergoing VPT when exposed to a DXP solution, where red and blue colours emanating from the shell are visible on the second image from the left taken after 0.5 min. During later stages of the volume transition, the collapsed phase relocated to a "cap" on one side of the microgels (third image from the left); in the rightmost image the VPT is completed. A similar phenomenon was previously reported for AMT – PA (Al-Tikriti and Hansson, 2022).

Dense shells may lower the drug transport rate inside microgels. In particular, during loading of highly charged proteins and self-assembling proteins, shells have been found to severely affect the kinetics (Wanselius, 2022; Andersson and Hansson, 2018; Johansson et al., 2009). However, in the case of amphiphilic molecules, where the transport through the shell is managed by small, low-charged monomers in local equilibrium with micelles, the transport even through very dense shells may not be rate-limiting during a large portion of the deswelling process (Nilsson and Hansson, 2005; Wanselius, 2022; Nilsson and Hansson, 2007; Nilsson and Hansson, 2008). Nevertheless, DC and PA exposed to the same concentrations of AMT, DXP, and CPZ have very different collapse rates in the second phase of collapse (Fig. 4), despite their similar CCCs. The charged networks in PA and DC have the same (high) linear charge density, and both microgels gain a core–shell structure during collapse. However, the difference between them is explained by the uncharged PVA chains in DC that effectively hinders a very strong collapse of the network, and so the shells are more swollen than for PA and therefore constitute a smaller diffusion barrier during the later stages when transport through the shell becomes rate determining. The difference was especially clear at exposure to DXP, where the time to reach the fully collapsed state for DC was ca. 2 min at all

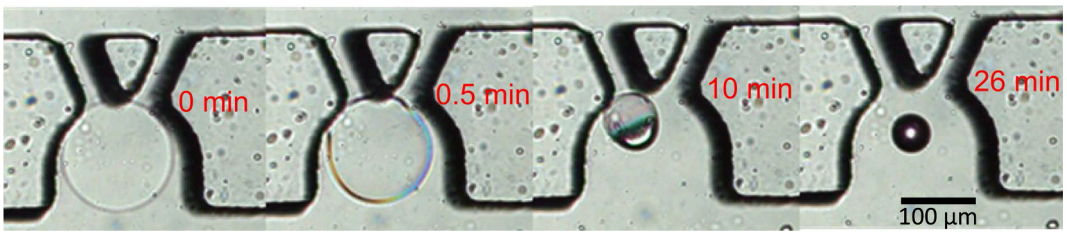

Fig. 5. Evolution of a PA undergoing VPT at exposure to 1.2 mM DXP solution. Colored reflections at edges (2nd image from the left; 0.5 min) indicates a collapsed shell of thickness comparable to the wavelength of visible light. At later stages the dense phase first relocates to a cap on one side of the microgel and finally occupies the entire microgel volume (3rd and 4th images from the left).

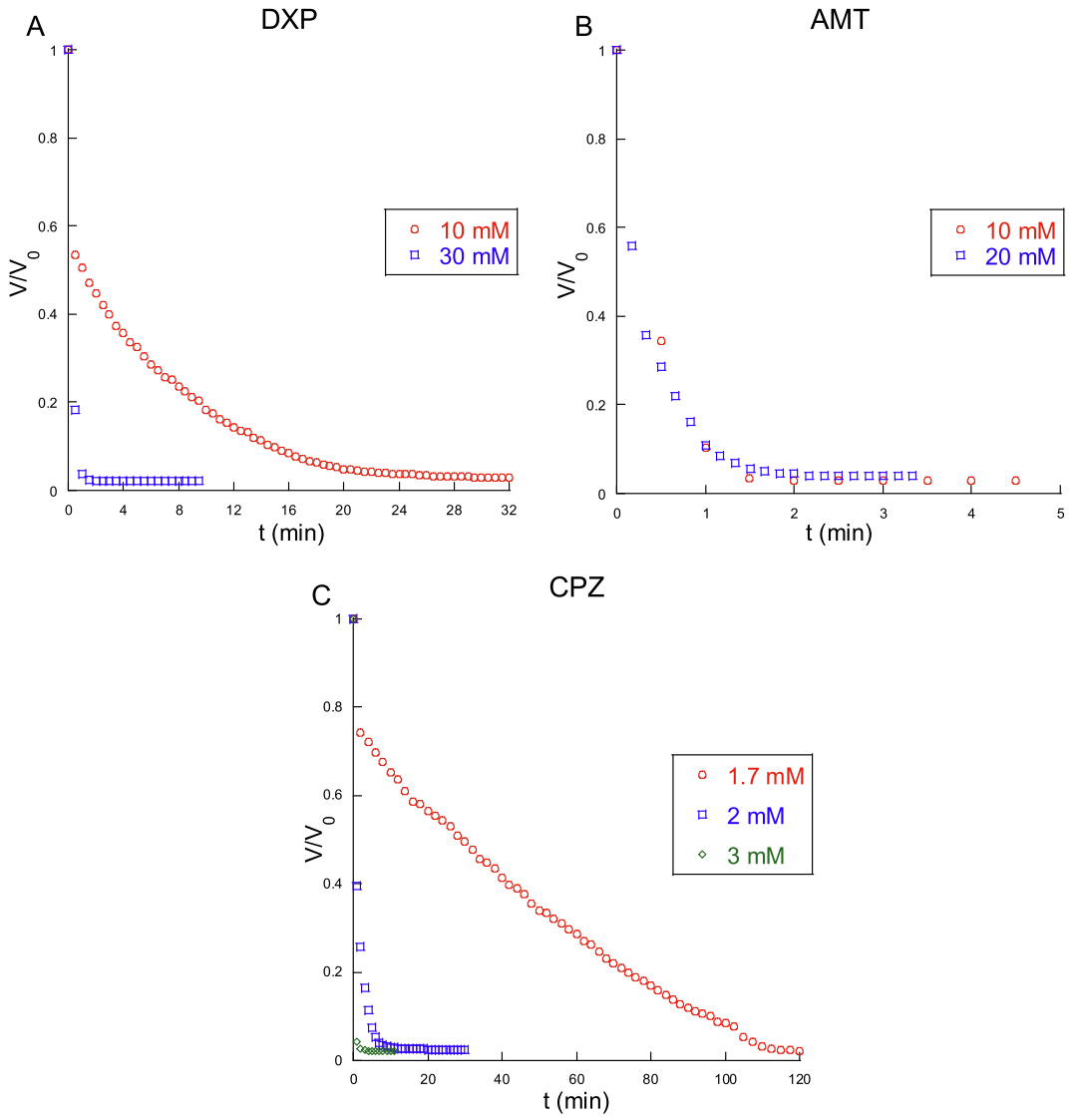

Fig. 6. Volume change of HA over time at exposure to DXP (A), AMT (B) and CPZ (C).

concentrations, while 12–15 min for PA.

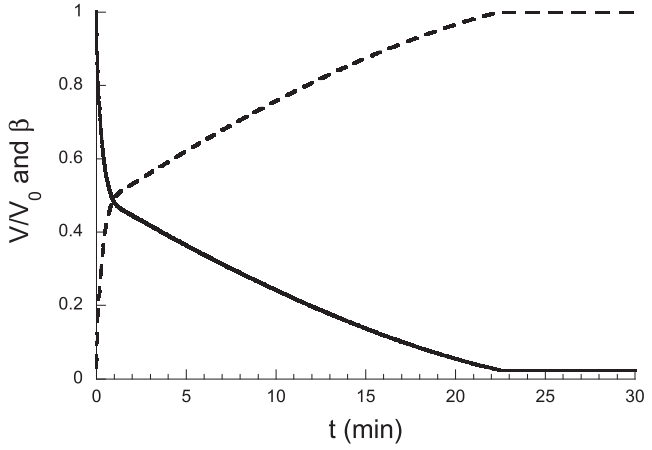

Fig. 7. Theoretically calculated volume ratio V/V_0 (solid curve) and binding ratio β (dashed curve) as functions of time during loading of a drug at a concentrations just above CCC for a model microgel with $R_0 = 70$ μm and $\bar{v}_0 = 0.018$ m^3/mol.

Fig. 6 shows deswelling profiles for the HA systems. In all cases the initial deswelling was very fast because the concentration in the liquid was well above CAC. However, fits of Eq. (1) to the data indicate that the process was not rate limited by stagnant layer diffusion (not shown). Interestingly, in the cases of 10 mM DXP and 1.7 mM CPZ, the rapid initial collapse was abruptly interrupted and replaced by a much slower deswelling process. Common to both cases is that the concentration in the liquid was very close to the concentration C_{liq}^{end} required to reach the fully collapsed state. The equilibrium swelling isotherm for CPZ has a region with a very steep slope but there was no obvious sign of VPT in that system or the HA/DXP system, nor was there a visually detectable core–shell separation (*cf.* Fig. 3C). However, the swelling isotherms for both systems are characteristic of cooperative binding. Hence, by taking into account also the comparatively weak electrostatic interaction between the drug aggregates and the weakly charged hyaluronic acid chains, it is possible that the drugs rapidly redistributed and maintained a fairly uniform distribution inside the microgels during binding. A possible scenario in such a case is that the drug concentration in the liquid, in local equilibrium with the microgel, initially remains much lower than the concentration in the bulk. During this stage, binding and deswelling is fast because of the large concentration gradient in the stagnant layer. However, rather than being fixed to a critical value (CCC), as when core–shell phase separation starts at low binding ratios

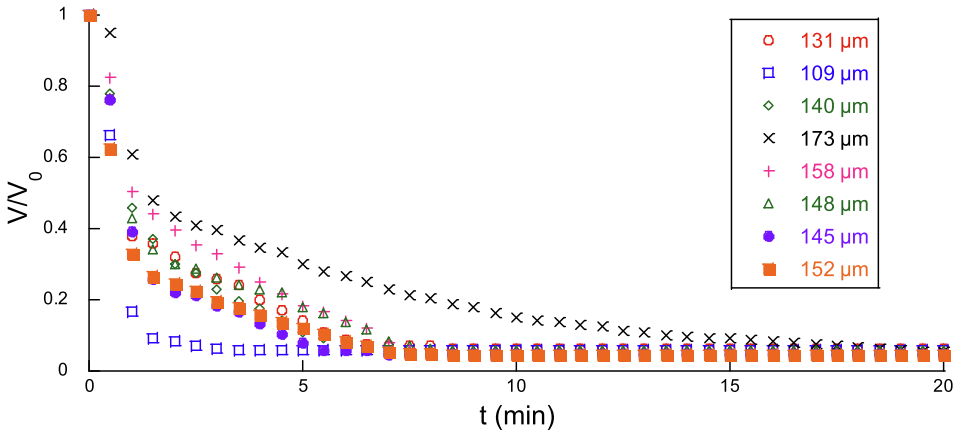

Fig. 8. Effect of initial gel diameter in PB (see legend) on the collapse kinetics of the PA exposed to DXP 1.2 mM.

(β), the local equilibrium concentration increases during the course of binding. This lowers the concentration gradient in the stagnant layer, hence slowing down the binding rate. The effect will be very pronounced if the local equilibrium concentration reaches a value very close to the bulk concentration. Now, if that takes place at the steepest part of the binding isotherm (near C_{liq}^{end}) or where a VPT takes place, binding and thus deswelling will continue but at a very low rate. To test this hypothesis we combined the kinetic expression for a stagnant layer-controlled process, Eq. (S:5), with information from theoretically calculated swelling and binding isotherms published in a previous paper (Wanselius, 2022). Specifically, we used the data behind the swelling isotherm at 20 mM salt in Fig. 9B in that paper, valid for an amphiphile with aggregation number 30 inside the microgel and with a CMC approximately equal to that of AMT. The microgel remains in a homogeneous (semi) swollen state for drug concentrations up to 10.10 mM, where a VPT to the fully collapsed state takes place; in the swollen phase at the transition point, β=0.51 and V/V_0 = 0.46. Fig. 7 shows the calculated deswelling profile for a microgel with R_0 = 70 μm and$\bar{v}_0$ = 0.018 m^3/mol in a solution withC^{liq} = 10.11 mM, Sh = 30, and $D = 4 \times 10^{-10}$ m^2/s. The result is in qualitative agreement with the experimental data for 10 mM DXP and 1.7 mM CPZ in Fig. 6.

Fig. 8 shows the effect of gel diameter on the collapse rate of PA exposed to 1.2 mM DXP, where a larger diameter can be seen to result in a slower collapse. This phenomenon, seen for the other gel types as well, can be explained by the larger amount of network charges in the gel. These charges need to be neutralized to reach a molar charge ratio $\beta \approx 1$, expected to be required for full collapse. The effect of size is clearest at bulk concentrations close to CCC where the rate of collapse is generally lower.

4.3. Swelling kinetics upon drug release

Swelling profiles for the three types of microgel during the release of the amphiphilic drugs in PB (7.4), 150 mM NaCl, are presented in Fig. 9 (PA, DC) and Fig. 10 (HA). Here, V_0 is defined as the volume of the microgels in PB (7.4), 150 mM NaCl, with no drug present.

For all gel types, a core–shell behaviour can be observed during swelling (Fig. 11), in agreement with earlier studies (Ahnfelt, 2018). In Fig. 12, the CAC values of AMT, DXP, and CPZ are plotted against the initial swelling rate k_s, determined as the slope of the initial part of the swelling curve. A higher CAC correlates with a more rapid release rate. This is in qualitative agreement with the mechanism proposed by Ahnfelt et al., in which the swelling rate depends on the drug concentration gradient in the depletion layer (Ahnfelt, 2018). The gradient increases with increasing monomer concentration at the core–shell interface, which is expected to increase with increasing CAC (or CMC).

In Fig. 12, the effect of charge concentration of the microgels is also evident. Thus, PA has the lowest swelling rates for all three drugs, followed by DC and finally the low-charged HA. The effect of microgel size is shown in Fig. 13A, where DC swelling during the release of CPZ is presented. The swelling rate decreased with increasing initial microgel diameter, as expected since the amount of drug loaded onto the microgel as well as the diffusion length inside the gel increases with increasing diameter. Fig. 13B shows that all swelling profiles collapse on a single master curve when the time scale is normalized by R_0^2, as suggested by Eq. (2). It shows that the theory provides a good description of the size dependence.

The release profiles also depended on the drug concentration in the liquid during loading. Higher concentration leads to a longer time to complete the swelling process, most clearly seen for the release of AMT from DC and PA (Fig. 9) where the largest concentration range was used. This can be explained by an increased drug load in the microgels with increasing concentration in the solution during loading. Thus, the higher the drug load, the longer the time to achieve complete release. Earlier work shows that binding isotherms tend to saturate when the binding ratio β approaches unity, but binding generally continues to increase slowly with increasing concentration in the solution, and binding ratios well above unity have been reported (Lewis, 2006). According to the release model for systems displaying a core–shell separation, Eq. (2), the release rate depends on the local binding ratio β_C in the core. To test this, we used binding data for the PA-AMT system, recently determined by Al-Tikriti and Hansson (unpublished results), providing β as a function of the loading concentration. To calculate the swelling profiles we first fitted the model to the data for the 1 mM AMT case ($\beta_C = 0.85$), using C_{in}^0 and a as fitting parameters. We then calculated the swelling profiles for the concentrations 4, 7, and 20 mM AMT with β_C equal to 1.14, 1.22 and 1.57, respectively; all other parameters the same as for 1 mM AMT. We set R_0 to value relevant for each microgel, $\bar{v}_C$=6.67 $\times$ 10^{-4} m^3/mole (=$1/C_p^{end}$, Table 2), $\bar{v}_0$=5.78 $\times$ 10^{-3} m^3/mole (calculated from gel model), D'=4 $\times$ 10^{-10} m^2/s, and used the function $\frac{\bar{v}_S}{\bar{v}_C} = f(q_S)$ determined earlier for PA to calculate the integral in Eq. (4) (see S1 for details) (Al-Tikriti and Hansson, 2020). The result, shown in Fig. 14A, reveals that the shape of the calculated curves are in good agreement with experiments at low but not at high swelling ratios. However, the model accounts quite well for the dependence on the loading concentration.

To investigate if the model could account also for the variation in swelling profile for the different drugs, we fitted the model to the PA swelling curves obtained at the respective lowest concentration of CPZ, DXP, and AMT in Fig. 9A-C, using C_{in}^0 as the only fitting parameter. Here, we set $\bar{v}_C$ and R_0 to the values relevant for respective experimental system; all other parameters were the same as for the calculations in Fig. 14A. From the fits, shown in Fig. 14B, we found that the C_{in}^0 values for CPZ:AMT:DXP were related as 1:3.5:6.2, in accordance with the CMC

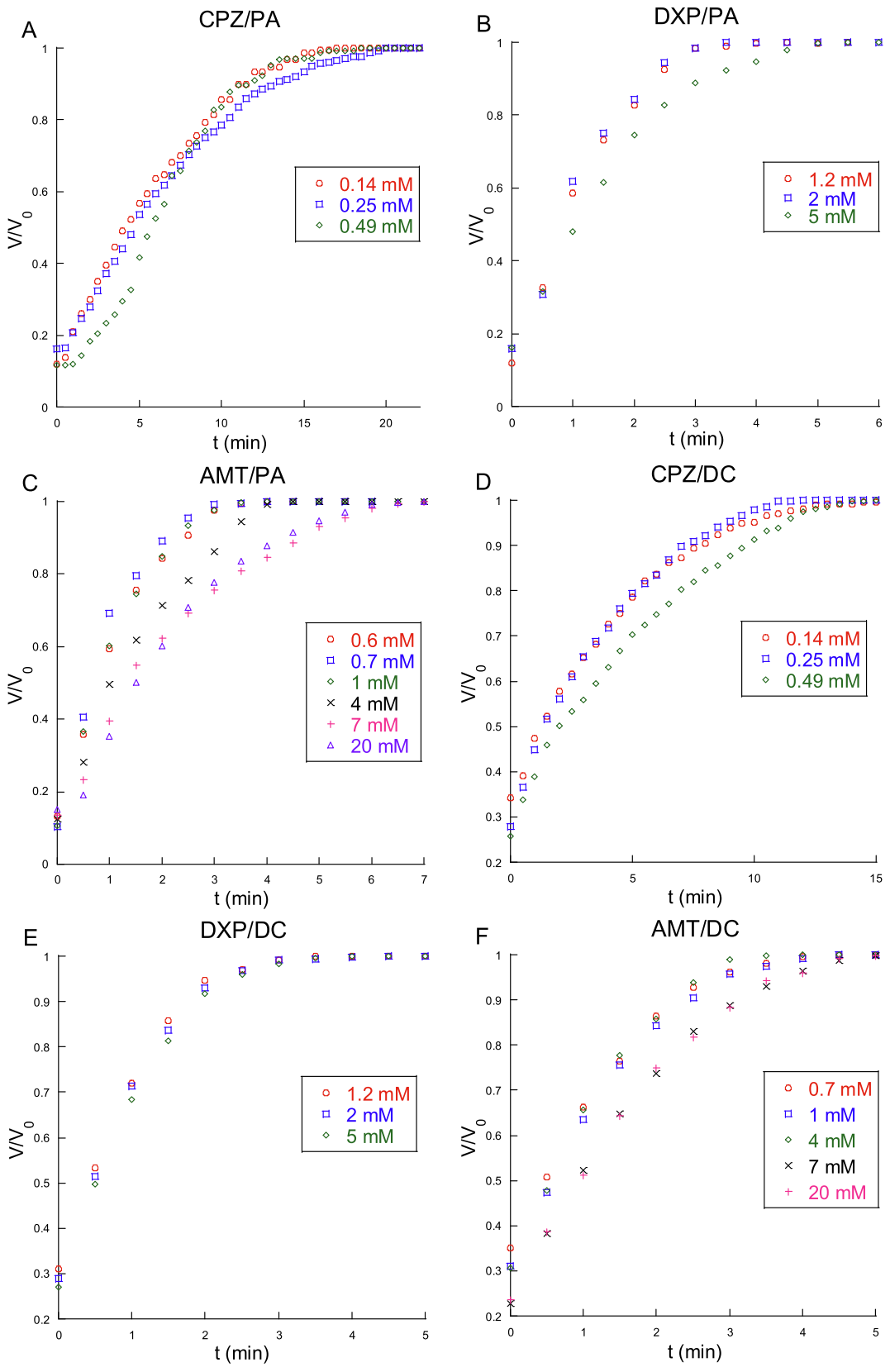

Fig. 9. Volume change of microgels during release of amphiphilic drugs. Release of CPZ (A), DXP (B) and AMT (C) from PA. Release of CPZ (D), DXP (E) and AMT (F) from DC.

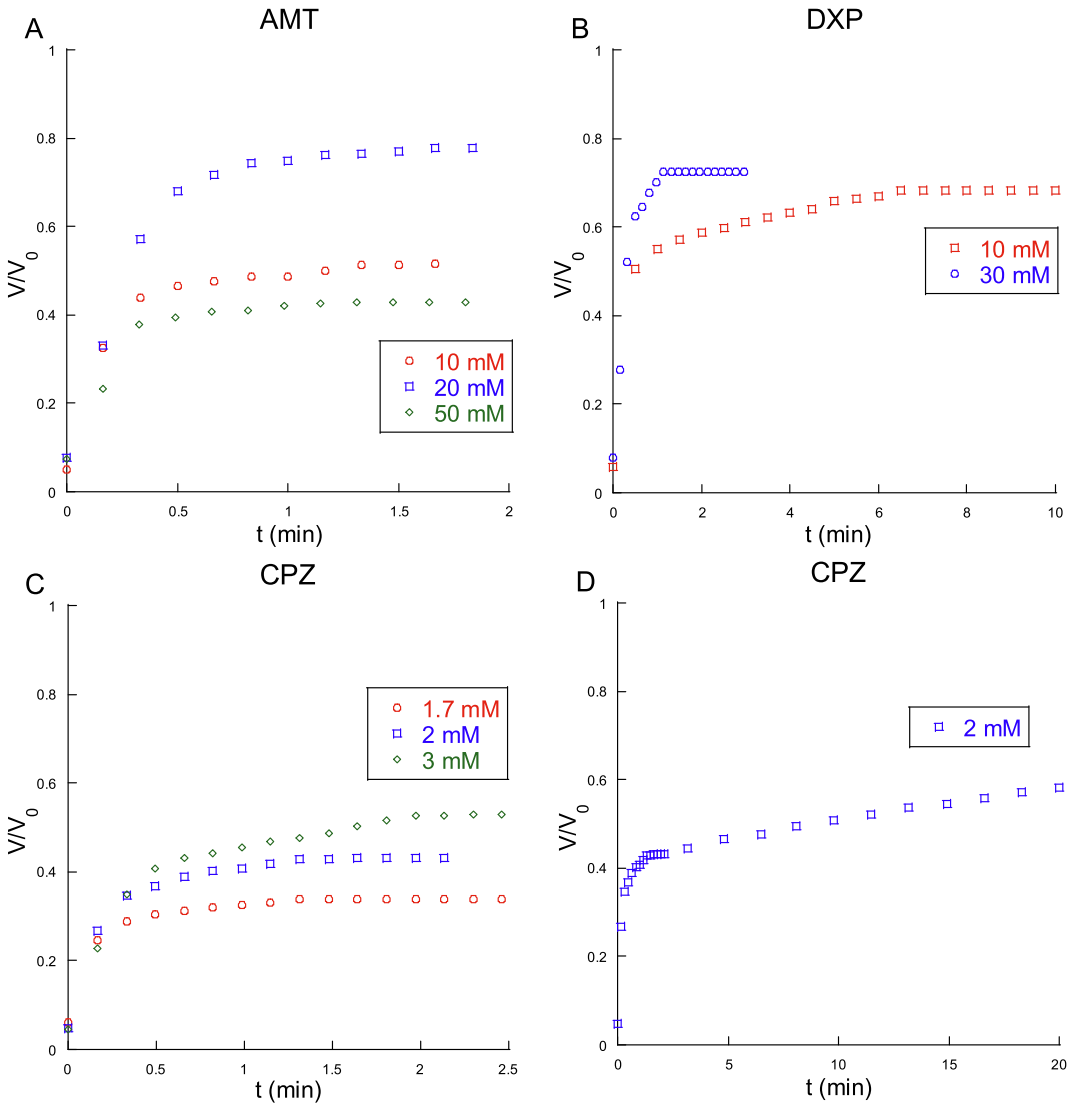

Fig. 10. Volume change of HA during release until an initial volume plateau for AMT (A), DXP (B), CPZ (C), and continued swelling long term over 20 min after release of CPZ (D).

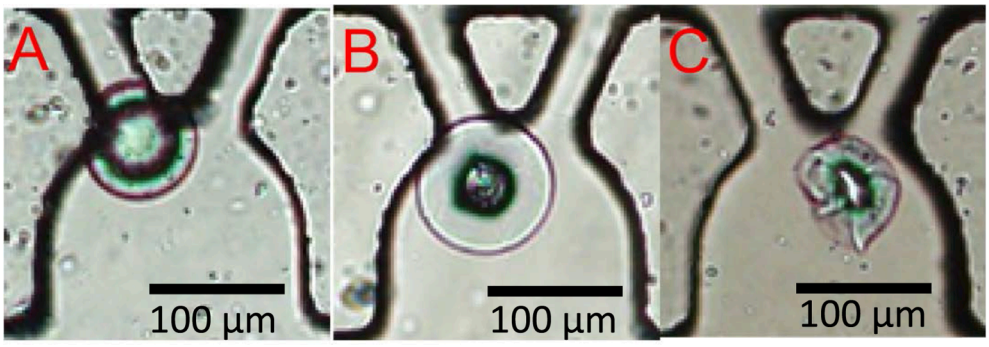

Fig. 11. Core shell structure during release of DXP from DC (A), PA (B), and HA (C).

values (Table 1). However, the relative difference between CPZ and AMT is smaller, and the relative difference between AMT and DXP is larger, than the corresponding differences in CAC (Table 3). One reason for the discrepancy could be that the CACs are valid for solutions with much lower ionic strength than in the release medium. Note also that C_{in}^{0} for DXP is more than double that for AMT, yet the swelling profiles nearly overlap. This is explained by the fact that R_0 for the PA used for DXP is larger than for AMT, and $\bar{v}_C$ is smaller for DXP than for AMT.

In conclusion, we have found that AMT, CPZ and DXP in combination with PA and DC behave, essentially, in agreement with the depletion layer model (Eq. (4) with respect to how the swelling rate depends on microgel size and charge content, the drugs' self-assembling tendencies,

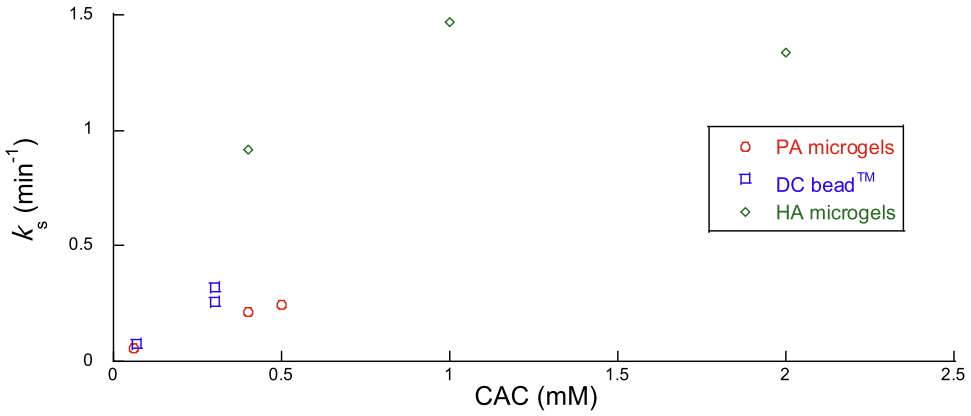

Fig. 12. Effect of CAC on the initial swelling rate k_s (min^{-1}) of microgels during release of amphiphilic drugs.

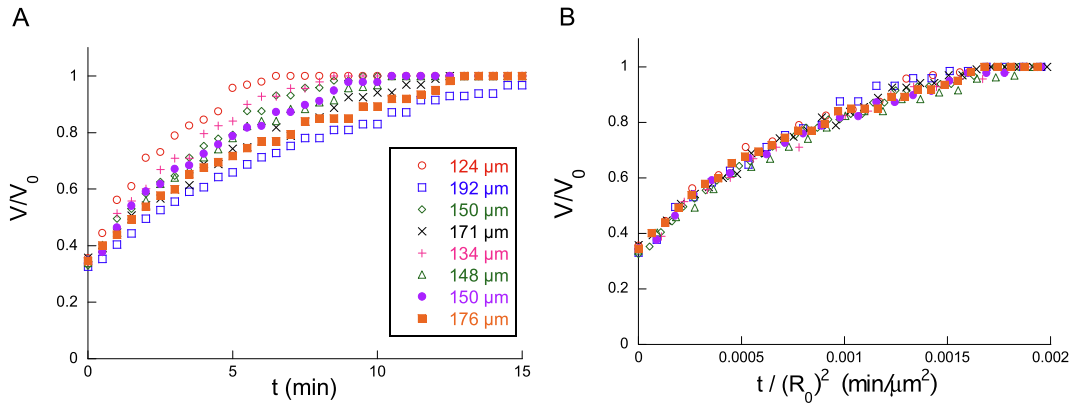

Fig. 13. A. Effect of initial DC diameter (see legend) on swelling profiles during release of CPZ in PB (7.4), 150 mM NaCl. B. The data in fig. A plotted on reduced time scale; R_0 is the initial radius.

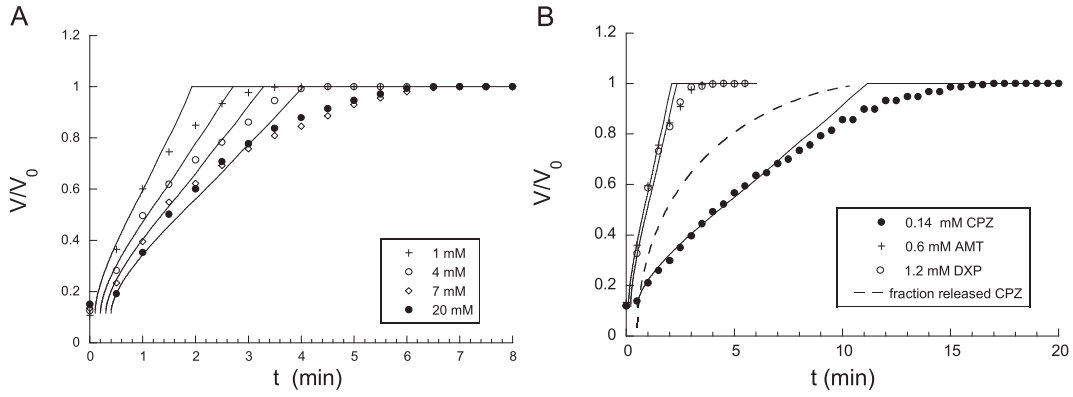

Fig. 14. Comparison of experimental (symbols) and theoretically calculated (solid curves) swelling profiles for PA releasing drug. A. Dependence on AMT loading concentration. B. Comparison between CPZ, AMT and DXP. Dashed curve is the calculated fractional release of CPZ. Experimental data from Fig. 9A-C. The curves have been adjusted horizontally to account for a short lag time.

and amount of drug loaded onto the microgels. This gives strong support to the basic assumption in the derivation of the model that drug mass transport is controlling the rate of swelling, and thus that the time for a microgel to reach the fully swollen state equals the time to release the drug loaded onto it. Implicitly, this means that all other processes, e.g., dissolution of micelles at the core–shell boundary, the relaxation of the polymer network, and re-establishing osmotic equilibrium with the surroundings, occur on shorter time scales. However, because the swelling response is not linearly dependent on the amount of drug released, the swelling profile does not directly reflect the release profile. This is illustrated in Fig. 14B, where we have plotted the calculated fraction released for CPZ corresponding to the swelling profile for the drug (dashed curve).

During release, PA and DC microgels swelled gradually following a single uninterrupted process until they regained the volume they had in PB (7.4), 150 mM NaCl, prior to drug binding. This was not the case for HA, where the swelling could be divided into a fast initial process followed by a very slow process. One example is the swelling accompanying the release of DXP presented in Fig. 10D, where a first rapid process during which the volume ratio reached 0.43 in less than 2 min,

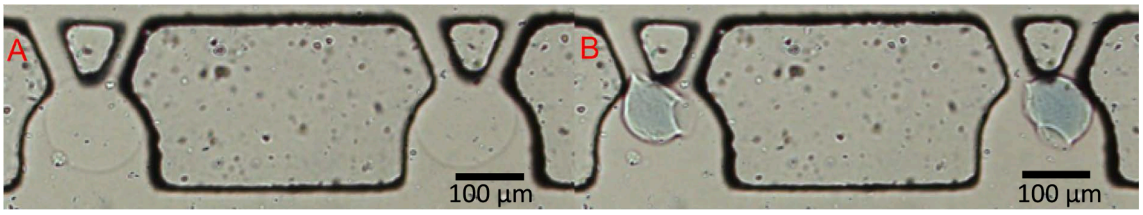

Fig. 15. HA before (A) and after (B) binding and release of DXP 30 mM.

was followed by a slow process during which it took 18 min to increase the volume ratio to 0.58. In fact, in none of the HA experiments did the microgels return to the size they had in the drug-free medium prior to binding during the time frame of our experiments. The reason for that is not clear but one may speculate that HA chains became more entangled in the collapsed state or that new crosslinks formed between unreacted ethyl acrylamide groups. The production of HA is performed by first modifying hyaluronic acid chains by exchanging a fraction of carboxylic acid groups with ethyl acrylamide groups and then using UV-light at 365 nm to crosslink the chains together. A characterization of the microgels, described elsewhere, showed that even at the low ethyl acrylamide modification degree of 13 % used in this work, there is likely a number of unreacted ethyl acrylamide groups on the hyaluronic acid chains (Wanselius et al., 2022). It is possible that these could have reacted with each other in the collapsed microgels where they are in close proximity to each other, which would modify the network structure and affect both the final volume and the swelling rate. Permanent changes of that type could perhaps explain why some microgels did not maintain a spherical shape (Fig. 15). Large variations in end volume make it difficult to reach clear conclusions about differences in release rate between different systems and the effect of loading concentration on the release rate.

5. Conclusions

In this work, we have utilized a highly efficient microfluidic setup, recently developed in our lab, to characterize a set of drug eluting microgel systems of potential use in parenteral drug administration (Wanselius, 2022). The results show that it is possible to load substantial amounts of AMT, CPZ and DXP onto the commercially available DC bead^{TM} system as well as onto PA and HA microgels made in house. Upon loading from a medium with low ionic strength the volume of microgels decreased dramatically in a way characteristic of amphiphilic molecules forming micelle-like aggregates in complex with oppositely charged networks, which at least for AMT and CPZ binding to PA involved a volume phase transition. The fully loaded microgels released their drug cargo when exposed to a medium with physiological ionic strength, a process accompanied by swelling of the microgel network. Our results show that the loading and release mechanisms resemble mechanism observed in the thoroughly investigated systems PA microgel + cationic surfactant as well as observed *in vitro* in the system DCbead^{TM} + doxorubicin (Ahnfelt, 2018) used in clinical treatments of liver cancer (Lewis and Holden, 2011). In particular, we show that the release obeyed the depletion layer mechanism proposed by Ahnfelt et al. in which the release rate is strongly influenced by the stability of the drug's self-assemblies in the microgel and the swelling properties of the network (Ahnfelt, 2018). This is significant because those properties can be used to control release rates and release profiles, highlighting the potential of microgels of the present type to be used as drug delivery systems. In this respect the results for HA microgels are particularly interesting because HA is biodegradable and considered biocompatible. However, the observation that the elasticity of the HA microgels decreased after the drug-induced collapse shows that the there is room for improvement of the microgel fabrication protocol. From a general methodological view point we conclude that our microfluidic platform can provide a large amount of experimental data in a time and material-efficient way, enabling extensive statistical analysis based on a few numbers of experiments, and is deemed suitable in a setup for high throughput screening of new microgel-based formulations systems.

CRediT authorship contribution statement

Marcus Wanselius: Conceptualization, Methodology, Validation, Formal analysis, Investigation, Writing – original draft, Visualization, Project administration. **Yassir Al-Tikriti:** Conceptualization, Investigation, Formal analysis, Writing – review & editing. **Per Hansson:** Conceptualization, Methodology, Formal analysis, Writing – original draft, Visualization, Supervision, Project administration, Funding acquisition.

Declaration of Competing Interest

The authors declare that they have no known competing financial interests or personal relationships that could have appeared to influence the work reported in this paper.

Data availability

Data will be made available on request.

Acknowledgments

This study is part of the science program of the Swedish Drug Delivery Center (SweDeliver) and financial support from Vinnova (Dnr 2019-00048) is gratefully acknowledged. Special thanks are given to Enas Bani Al-Marjeh for her help with the image analysis.

Appendix A. Supplementary material

Supplementary data to this article can be found online at https://doi.org/10.1016/j.ijpharm.2023.123517.

References

Ahmad, S.A., Lewis, A.L., Parkes, G., Tang, Y., Waters, L.J., 2021. Quantification and characterization of water within drug-eluting beads. Polymer 235, 124287.
Ahnfelt, E., et al., 2018. Single bead investigation of a clinical drug delivery system – A novel release mechanism. J. Control. Release 292, 235–247.
Al-Tikriti, Y., Hansson, P., 2020. Drug-Eluting Polyacrylate Microgels: Loading and Release of Amitriptyline. J. Phys. Chem. B 124, 2289–2304.
Al-Tikriti, Y., Hansson, P., 2022. Drug-Induced Phase Separation in Polyelectrolyte Microgels. Gels 8.
am Ende, M.T., Peppas, N.A., 1997. Transport of ionizable drugs and proteins in crosslinked poly(acrylic acid) and poly(acrylic acid-co-2-hydroxyethyl methacrylate) hydrogels. II. Diffusion and release studies. J. Control. Release 48, 47–56.
Andersson, M., Hansson, P., 2017. Phase Behavior of Salt-Free Polyelectrolyte Gel-Surfactant Systems. J. Phys. Chem. B 121, 6064–6080.
Andersson, M., Hansson, P., 2018. Binding of Lysozyme to Spherical Poly (styrenesulfonate) Gels. Gels 4, 9.
Attwood, D., Gibson, J., 1978. Aggregation of antidepressant drugs in aqueous solution. J. Pharm. Pharmacol. 30, 176–180.
Attwood, D., Natarajan, R., 1983. Micellar properties of chlorpromazine hydrochloride in concentrated electrolyte solutions. J. Pharm. Pharmacol. 35, 317–319.
Censi, R., Di Martino, P., Vermonden, T., Hennink, W.E., 2012. Hydrogels for protein delivery in tissue engineering. J. Control. Release 161, 680–692.

Cleland, J.L., Johnson, O.L., Putney, S., Jones, A.J.S., 1997. Recombinant human growth hormone poly(lactic-co-glycolic acid) microsphere formulation development. Adv. Drug Deliv. Rev. 28, 71–84.
Efthymiou, C., Bergström, L.M., Pedersen, J.N., Pedersen, J.S., Hansson, P., 2021. Self-assembling properties of ionisable amphiphilic drugs in aqueous solution. J. Colloid Interface Sci. 600, 701–710.
Eichenbaum, G.M., Kiser, P.F., Dobrynin, A.V., Simon, S.A., Needham, D., 1999. Investigation of the swelling response and loading of ionic microgels with drugs and proteins: The dependence on cross-link density. Macromolecules 32, 4867–4878.
Embil, K., Torosian, G., 1982. Solubility and Ionization Characteristics of Doxepin and Desmethyldoxepin. J. Pharm. Sci. 71, 191–193.
Evans, F., Wennerström, H., 1994. The Colloidal Domain: where Physics, Chemistry, Biology, and Technology Meet. VCH Publishers.
Gernandt, J., Hansson, P., 2015. Hysteresis in the surfactant-induced volume transition of hydrogels. J. Phys. Chem. B 119, 1717–1725.
Gernandt, J., Hansson, P., 2016. Surfactant-induced core/shell phase equilibrium in hydrogels. J. Chem. Phys. 144, 064902.
Green, A.L., 1967. Ionization constants and water solubilities of some aminoalkylphenothiazine tranquillizers and related compounds. J. Pharm. Pharmacol. 19, 10–16.
Hagan, A., et al., 2019. Predicting pharmacokinetic behaviour of drug release from drug-eluting embolization beads using in vitro elution methods. Eur. J. Pharm. Sci. 136, 104943.
Hansson, P., 1998. Surfactant self-assembly in polyelectrolyte gels: Aggregation numbers and their relation to the gel collapse and the appearance of ordered structures in the NaPA/C12TAB system. Langmuir 14, 4059–4064.
Hansson, P., 2006. Interaction between polyelectrolyte gels and surfactants of opposite charge. Curr. Opin. Colloid Interface Sci. 11, 351–362.
Hansson, P., 2009. Surfactant self-assembly in oppositely charged polymer networks. Theory. J. Phys. Chem. B 113, 12903–12915.
Hansson, P., 2020. Volume transition and phase coexistence in polyelectrolyte gels interacting with amphiphiles and proteins. Gels 6, 24.
IJzerman, A.P., 1988. Limiting Solubilities and Ionization Constants of Sparingly Soluble Compounds: Determination from Aqueous Potentiometric Titration Data Only. Pharm. Res. 5, 772–775.
Jain, D., Mahammad, S.S., Singh, P.P., Kodipyaka, R., 2019. A review on parenteral delivery of peptides and proteins. Drug Dev. Ind. Pharm. 45, 1403–1420.
Johansson, C., Hansson, P., Malmsten, M., 2009. Mechanism of lysozyme uptake in poly (acrylic acid) microgels. J. Phys. Chem. B 113, 6183–6193.
Kabanov, V.A., Zezin, A.B., Rogacheva, V.B., Khandurina, Y.V., 1997. Absorption of ionic amphiphils by oppositely charged polyelectrolytes. Macromol. Symp. 126, 79–94.
Karg, M., et al., 2019. Nanogels and Microgels: From Model Colloids to Applications, Recent Developments, and Future Trends. Langmuir 35, 6231–6255.
Khandurina, Y.V., Dembo, A.T., Rogacheva, V.B., Zezin, A.B., Kabanov, V.A., 1994. Structure of polycomplexes composed of cross-linked sodium polyacrylate and cationic micelle-forming surfactants. Polym. Sci. 36, 189–194.
Khokhlov, A.R., Kramarenko, E.Y., Makhaeva, E.E., Starodoubtzev, S.G., 1992. Collapse of polyelectrolyte networks induced by their interaction with an oppositely charged surfactant. Theory. Makromol. Chem. Theory Simul. 1, 105–118.
Kim, S.J., Hahn, S.K., Kim, M.J., Kim, D.H., Lee, Y.P., 2005. Development of a novel sustained release formulation of recombinant human growth hormone using sodium hyaluronate microparticles. J. Control. Release 104, 323–335.
Lengyel, M., Kállai-Szabó, N., Antal, V., Laki, J.A., Antal, I., 2019. Microparticles, Microspheres, and Microcapsules for Advanced Drug Delivery. Sci. Pharm. 87.
Lewis, A.L., et al., 2006. DC Bead. In Vitro Characterization of a Drug-delivery Device for Transarterial Chemoembolization. J. Vasc. Interv. Radiol. 17, 335–342.
Lewis, A.L., Dreher, M.R., 2012. Locoregional drug delivery using image-guided intra-arterial drug eluting bead therapy. J. Control. Release 161, 338–350.
Lewis, A.L., Holden, R.R., 2011. DC Bead embolic drug-eluting bead: Clinical applications in the locoregional treatment of tumors. Expert Opin. Drug Delivery 8, 153–169.
Malmsten, M., Bysell, H., Hansson, P., 2010. Biomacromolecules in microgels - opportunities and challanges for drug delivery. Curr. Opin. Colloid Interface Sci. 15, 435–444.
Mikhail, A.S., et al., 2021. Drug-eluting embolic microspheres: State-of-the-art and emerging clinical applications. Expert Opin. Drug Deliv. 18, 383–398.
Mikhail, A.S., et al., 2022. Evaluation of immune-modulating drugs for use in drug-eluting microsphere transarterial embolization. Int. J. Pharm. 616, 121466.
Murray, M.J., Snowden, M.J., 1995. The preparation, characterisation and application of colloidal microgels. Adv. Colloid Interface Sci. 54, 73–91.
Narayanaswamy, R., Torchilin, V.P., 2019. Hydrogels and Their Applications in Targeted Drug Delivery. Molecules 24, 603.
Nilsson, P., Hansson, P., 2005. Ion-exchange controls the kinetics of deswelling of polyelectrolyte microgels in solutions of oppositely charged surfactant. J. Phys. Chem. B 109, 23843–23856.
Nilsson, P., Hansson, P., 2007. Deswelling kinetics of polyacrylate gels in solutions of cetyltrimethylammunium bromide. J. Phys. Chem. B 111, 9770–9778.
Nilsson, P., Hansson, P., 2008. Regular and Irregular deswelling of polyacrylate and hyaluronate gels induced by oppositely charged surfactants. J. Colloid Int. Sci. 325, 316–323.
Patel, A., Cholkar, K., Mitra, K.A., 2014. Recent developments in protein and peptide parenteral delivery approaches. Ther. Deliv. 5, 337–365.
Perez-Villar, V., Vazquez-Iglesias, M.E., de Geyer, A., 1993. Small-angle neutron scattering studies of chlorpromazine micelles in aqueous solutions. J. Phys. Chem. B 97, 5149–5154.
Ran, R., et al., 2017. Multiphase microfluidic synthesis of micro- and nanostructures for pharmaceutical applications. Chem. Eng. Sci. 169, 78–96.
Sasaki, S., Koga, S., Imabayashi, R., Maeda, H., 2001. Salt effects on the volume transition of ionic gel induced by the hydrophobic counterion binding. J. Phys. Chem. B 105, 5852–5855.
Saunders, B.R., Crowther, H.M., Vincent, B., 1997. Poly[(methyl methacrylate)-co-(methacrylic acid)] microgel particles: Swelling control using pH, cononsolvency, and osmotic deswelling. Macromolecules 30, 482–487.
Schwendeman, S.P., Shah, R.B., Bailey, B.A., Schwendeman, A.S., 2014. Injectable controlled release depots for large molecules. J. Control. Release 190, 240–253.
Siepmann, J., Siepmann, F., 2012. Modeling of diffusion controlled drug delivery. J. Control. Release 161, 351–362.
Tanaka, T., 1978. Collapse of gels and the critical endpoint. Phys. Rev. Lett. 40, 820–823.
Tararyshkin, D., Kramarenko, E., Khokhlov, A.R., 2007. Two-phase structure of polyelectrolyte gel/surfactant complexes. J. Chem. Phys. 126, 164905.
Vinogradov, S.V., 2006. Colloidal microgels in drug delivery applications. Curr. Pharm. Des. 12, 4703–4712.
Wanselius, M., et al., 2022. Microfluidics platform for studies of peptide – polyelectrolyte interaction. Int. J. Pharm. 621, 121785.
Wanselius, M., Rodler, A., Searle, S.S., Abrahmsén-Alami, S., Hansson, P., 2022. Responsive Hyaluronic Acid-Ethylacrylamide Microgels Fabricated Using Microfluidics Technique. Gels 8, 588.
Wechsler, M.E., et al., 2019. Engineered microscale hydrogels for drug delivery, cell therapy, and sequencing. Biomed. Microdevices 21, 31.
Yeh, F., Sokolov, E.L., Walter, T., Chu, B., 1998. Structure studies of poly (diallyldimethylammonium chloride-co-acrylamide) gels/sodium dodecyl sulfate complex. Langmuir 14, 4350–4358.
Zhang, Y., Chan, H.F., Leong, K.W., 2013. Advanced materials and processing for drug delivery: The past and the future. Adv. Drug Deliv. Rev. 65, 104–120.